Variational Contact–Implicit Trajectory Optimization

Conference Paper · December 2017

2 authors, including:

Some of the authors of this publication are also working on these related projects:

Motion Planning View project

Discrete Mechanics View project

Variational Contact-Implicit Trajectory Optimization

Zachary Manchester and Scott Kuindersma

Abstract Contact constraints arise naturally in many robot planning problems. In recent years, a variety of *contact-implicit* trajectory optimization algorithms have been developed that avoid the pitfalls of mode pre-specification by simultaneously optimizing state, input, and contact force trajectories. However, their reliance on first-order integrators leads to a linear tradeoff between optimization problem size and plan accuracy. To address this limitation, we propose a new family of trajectory optimization algorithms that leverage ideas from discrete variational mechanics to derive higher-order generalizations of the classic time-stepping method of Stewart and Trinkle. By using these dynamics formulations as constraints in direct trajectory optimization algorithms, it is possible to perform contact-implicit trajectory optimization with significantly higher accuracy. For concreteness, we derive a second-order method and evaluate it using several simulated rigid body systems including an underactuated biped and a quadruped.

1 Introduction

Trajectory optimization algorithms comprise a powerful collection of methods for planning motions of nonlinear dynamical systems [3]. Generally speaking, these algorithms aim to find an input trajectory that minimizes a cost function subject to a set of constraints on the system's states and inputs. Trajectory optimization has a long history of successful application to systems with smooth dynamics. However, many robotic systems experience discontinuous frictional contact with the en-

Zachary Manchester

Harvard University, 60 Oxford St. Cambridge, MA 02138. e-mail: `zmanchester@seas.harvard.edu`

Scott Kuindersma

Harvard University, 33 Oxford St. Cambridge, MA 02138. e-mail: `scottk@seas.harvard.edu`

vironment as an essential part of their routine operation. The non-smooth dynamics encountered in these situations pose significant challenges.

A popular approach for handling contact events is to use a hybrid system model that explicitly accounts for discontinuities [20]. However, contact mode sequences must then be pre-specified by the user or generated by a higher-level heuristic planner. This approach can work quite well for systems with a small number of contacts [6, 14, 22, 21, 27]. Unfortunately, for more complex systems, the number of modes grows exponentially with the number of contact constraints, making mode sequence pre-specification computationally impractical.

Recently, an alternative approach has emerged in which state, input, and contact force trajectories are simultaneously optimized [19, 15, 25]. These so-called *contact-implicit* trajectory optimization methods can synthesize motions without *a priori* specification of the contact mode sequence. However, current state-of-the-art algorithms rely on first-order discretizations of the dynamics constraints, severely limiting accuracy and closed-loop trajectory tracking performance [27, 20].

To overcome the accuracy limitations of current algorithms, we propose a new family of *variational* contact-implicit methods that combine ideas from discrete variational mechanics with the complementarity formulation of rigid body contact to achieve higher-order integration accuracy. For simplicity and concreteness, we provide an explicit derivation of a second-order method. However, the mathematical tools used are general, and can be applied to derive integrators of arbitrary order.

The remainder of the paper is organized as follows: Section 2 provides a summary of related work on trajectory optimization through contact. Section 3 then gives a brief review of some important concepts from both classical variational mechanics and discrete mechanics. Section 4 derives the new variational rigid body time-stepping scheme, and Section 5 introduces a direct trajectory optimization algorithm built around these dynamics. Several examples that demonstrate the performance of the new algorithm are then presented in Section 6. Finally, we summarize our findings in Section 7.

2 Related Work

In spite of their limitations, hybrid trajectory optimization algorithms that rely on a pre-specified contact mode sequence have had a number of notable successes. For example, hybrid multiple-shooting algorithms have been used to find open-loop stable walking trajectories for a two-dimensional model of a humanoid [14] and to study the energetics of quadrupedal locomotion [21]. Hybrid collocation methods with third-order integration accuracy have also been demonstrated on a full-body model of a humanoid [20].

Much of the recent work on contact-implicit methods has focused on approximation schemes to smooth discontinuities. Several authors have developed indirect trajectory optimization algorithms based on differential dynamic programming (DDP) [13] that apply a smoothing function to the contact constraints [25] or penal-

ize constraint violations in the objective function [26, 10]. The penalty approach has also been applied in direct trajectory optimization methods [15]. These algorithms have been used to plan motions for quadrupeds [10] and simplified humanoids [26, 25, 15] in simulation.

Another method for handling contact in trajectory optimization algorithms is to use a spring-and-damper model to generate contact forces. Such approaches often require very large values of spring and damping constants to achieve realistic behavior, necessitating very small step sizes [23]. However, Neunert et. al. [9] have reported positive results using a nonlinear spring-and-damper model as part of a DDP-based algorithm. Their work is particularly notable for its successful demonstration in hardware experiments on a quadrupedal robot.

The previous work most closely related to the present paper is that of Posa, Cantu, and Tedrake [19]. Their algorithm attempts to accurately capture discontinuous rigid-body physics by relying on the "time-stepping" linear complementarity formulation of Stewart and Trinkle [24, 2]. The essential idea behind time-stepping methods for simulating rigid-body dynamics is to apply a first-order semi-implicit Euler discretization to the dynamics,

$$M(q_k)(v_{k+1} - v_k) = h\left(B(q_k)u_k + N(q_k)^T\gamma_k - C(q_k, v_{k+1})\right)$$
$$q_{k+1} = q_k + hv_{k+1},$$
(1)

where k is a time index; q, v, u, and γ are configurations, velocities, control inputs, and normal contact impulses acting over a timestep of length h, respectively; M is the system's mass matrix; B and N^T are the Jacobians mapping control inputs and normal contact forces into generalized coordinates; and C includes Coriolis and potential terms. We have temporarily ignored the tangental (friction) component of the contact force for clarity, but it is discussed extensively in Section 4.2). For the normal component, we have the following constraints:

$$\gamma_k \geq 0$$
$$\phi(q_{k+1}) \geq 0$$
$$\gamma_k\phi(q_{k+1}) = 0,$$
(2)

where $\phi(q)$ is a function that returns the signed distance between closest points on bodies.

In words, the conditions in equation (2) specify that normal forces can only push bodies apart (not pull them together), that bodies cannot interpenetrate, and that contact forces can only be non-zero when bodies are in contact. The combination of (1) and (2) forms a linear complementarity problem (LCP) that can be solved efficiently [2]. However, this formulation depends crucially on the particular choice of first-order discretization used in (1). While it may be possible to apply a higher-order discretization scheme in an *ad hoc* way, it is not obvious how to do so while still satisfying the contact constraints. To overcome this, the next few sections introduce a set of mathematical tools for systematically deriving time-stepping methods with any desired order of integration accuracy.

3 Preliminaries

This section reviews some classical results from variational mechanics, as well as some more recent results from discrete mechanics.

3.1 Lagrange-D'Alembert Principle

Our starting point is the Lagrange-D'Alembert principle, which is the integral form of D'Alembert's principle of virtual work [11], and can also be thought of as a modification of Hamilton's principle of least action to accommodate external forces:

$$\delta \int_{t_0}^{t_f} \mathscr{L}(q, \dot{q}) \, dt + \int_{t_0}^{t_f} F \cdot \delta q \, dt = 0. \tag{3}$$

We use $\mathscr{L}$ to denote the system's Lagrangian, F to denote a generalized force, and δ to indicate a variation. Equation (3) describes a boundary-value problem in which a trajectory $q(t)$ is sought given fixed end points $q(t_0)$ and $q(t_f)$.

We now review the steps used to derive the classical forced Euler-Lagrange equation from (3). Carrying out the variational derivative results in,

$$\int_{t_0}^{t_f} D_1\mathscr{L}(q, \dot{q}) \cdot \delta q + D_2\mathscr{L}(q, \dot{q}) \cdot \delta \dot{q} \, dt + \int_{t_0}^{t_f} F \cdot \delta q \, dt = 0, \tag{4}$$

where we have used the *slot derivative D_i* to indicate partial differentiation with respect to a function's i^{th} argument. The next step is to eliminate $\delta \dot{q}$ by performing an integration by parts:

$$\int_{t_0}^{t_f} D_1\mathscr{L}(q, \dot{q}) \cdot \delta q - \frac{d}{dt} D_2\mathscr{L}(q, \dot{q}) \cdot \delta q \, dt + \int_{t_0}^{t_f} F \cdot \delta q \, dt$$
$$+ D_2\mathscr{L}(q(t_f), \dot{q}(t_f)) \cdot \delta q(t_f) - D_2\mathscr{L}(q(t_0), \dot{q}(t_0)) \cdot \delta q(t_0) = 0. \tag{5}$$

The fact that the end points $q(t_0)$ and $q(t_f)$ of the boundary value problem are fixed, and thus $\delta q(t_0) = \delta q(t_f) = 0$, can be used to eliminate the last two terms in (5):

$$\int_{t_0}^{t_f} D_1\mathscr{L}(q, \dot{q}) \cdot \delta q - \frac{d}{dt} D_2\mathscr{L}(q, \dot{q}) \cdot \delta q \, dt + \int_{t_0}^{t_f} F \cdot \delta q \, dt = 0. \tag{6}$$

Finally, recognizing that equation (6) must hold for all variations δq, we arrive at the forced Euler-Lagrange equation:

$$\frac{d}{dt} D_2\mathscr{L}(q, \dot{q}) - D_1\mathscr{L}(q, \dot{q}) = F. \tag{7}$$

3.2 Discrete Mechanics

Discrete mechanics encompasses a set of mathematical tools for deriving special-ized numerical integrators for mechanical systems. These so-called *variational integrators* have many advantages over traditional Runge-Kutta schemes, including realistic long-term energy and momentum behavior [12] (although this is not our primary focus).

The general strategy behind discrete mechanics is to approximate the integrals in (3) with a quadrature rule *before* taking variations. We begin by breaking those integrals into N smaller pieces,

$$\delta \sum_{k=0}^{N-1} \int_{t_k}^{t_{k+1}} \mathscr{L}(q,\dot{q})\,dt + \sum_{k=0}^{N-1} \int_{t_k}^{t_{k+1}} F(q,\dot{q}) \cdot \delta q\,dt = 0, \tag{8}$$

where $t_k = t_0 + kh$ and h is a small timestep. Each short integral in equation (8) is then approximated. For simplicity and concreteness, we will use the midpoint rule:

$$\delta \sum_{k=0}^{N-1} h\mathscr{L}\left(\frac{q_k + q_{k+1}}{2}, \frac{q_{k+1} - q_k}{h}\right)$$
$$+ \sum_{k=0}^{N-1} \frac{h}{2} F\left(\frac{q_k + q_{k+1}}{2}, \frac{q_{k+1} - q_k}{h}\right) \cdot (\delta q_k + \delta q_{k+1}) = 0. \tag{9}$$

Equation (9) can be written more compactly as,

$$\delta \sum_{k=0}^{N-1} \mathscr{L}_d(q_k, q_{k+1}) + \sum_{k=0}^{N-1} \frac{1}{2} F_d(q_k, q_{k+1}) \cdot (\delta q_k + \delta q_{k+1}) = 0, \tag{10}$$

where $\mathscr{L}_d$ is the discrete Lagrangian,

$$\mathscr{L}_d(q_k, q_{k+1}) = h\mathscr{L}\left(\frac{q_k + q_{k+1}}{2}, \frac{q_{k+1} - q_k}{h}\right), \tag{11}$$

and F_d is the discrete generalized force,

$$F_d(q_k, q_{k+1}) = hF\left(\frac{q_k + q_{k+1}}{2}, \frac{q_{k+1} - q_k}{h}\right). \tag{12}$$

Note that the definitions of the discrete Lagrangian and discrete generalized force depend on our choice of quadrature rule [12].

We now carry out the variational derivative in (10):

$$\sum_{k=0}^{N-1} D_1 \mathscr{L}_d(q_k, q_{k+1}) \cdot \delta q_k + D_2 \mathscr{L}_d(q_k, q_{k+1}) \cdot \delta q_{k+1}$$

$$+ \sum_{k=0}^{N-1} \frac{1}{2} F_d(q_k, q_{k+1}) \cdot (\delta q_k + \delta q_{k+1}) = 0. \quad (13)$$

Paralleling the derivation of the classical Euler-Lagrange equation in the previous section, we perform a "discrete integration by parts" to line up the time indices of the δq terms. This amounts to a simple index manipulation trick:

$$D_1 \mathscr{L}_d(q_0, q_1) \delta q_0 + \frac{1}{2} F_d(q_0, q_1) \cdot \delta q_0$$

$$+ \sum_{k=1}^{N-1} \left(D_2 \mathscr{L}_d(q_{k-1}, q_k) + D_1 \mathscr{L}_d(q_k, q_{k+1}) + \frac{1}{2} F_d(q_{k-1}, q_k) + \frac{1}{2} F_d(q_k, q_{k+1}) \right) \cdot \delta q_k$$

$$+ D_2 \mathscr{L}_d(q_{N-1}, q_N) \delta q_N + \frac{1}{2} F_d(q_{N-1}, q_N) \cdot \delta q_N = 0. \quad (14)$$

As in the continuous case, the endpoints q_0 and q_N are fixed. As a result, $\delta q_0 = \delta q_N = 0$, and the first and last terms in (14) can be eliminated:

$$\sum_{k=1}^{N-1} \left(D_2 \mathscr{L}_d(q_{k-1}, q_k) + D_1 \mathscr{L}_d(q_k, q_{k+1}) \right.$$

$$\left. + \frac{1}{2} F_d(q_{k-1}, q_k) + \frac{1}{2} F_d(q_k, q_{k+1}) \right) \cdot \delta q_k = 0. \quad (15)$$

Finally, using the fact that equation (15) must hold for all variations δq_k, we arrive at the following discrete-time version of the forced Euler-Lagrange equation:

$$D_2 \mathscr{L}_d(q_{k-1}, q_k) + D_1 \mathscr{L}_d(q_k, q_{k+1}) + \frac{1}{2} F_d(q_{k-1}, q_k) + \frac{1}{2} F_d(q_k, q_{k+1}) = 0. \quad (16)$$

Equation (16) can be used to simulate the dynamics of a mechanical system by inserting values for q_{k-1} and q_k and solving for q_{k+1}. In fact, it is equivalent to the implicit midpoint method. In general, the order of accuracy of a variational integrator is equal to the order of accuracy of the quadrature rule used in its construction [12]. Since the midpoint rule has a global error of $O(h^2)$, an integrator based on (16) inherits this second-order accuracy. Variational integrators of any desired order can be derived by simply choosing an appropriate quadrature rule [18].

4 Variational Time-Stepping Methods

Time-stepping methods for simulating rigid body dynamics with contact were first proposed by Stewart and Trinkle [24]. The essential idea is to deal with the discon-

tinuities that occur during rigid body impacts by formulating the dynamics at the level of impulses and velocities, rather than forces and accelerations. The contact impulse produced during a timestep is computed, together with the next state, by solving a constrained optimization problem.

Since variational integrators like (16) are also formulated in terms of impulses and avoid direct computation of forces and accelerations, they are a natural choice for handling rigid body contact dynamics. In this section, we derive a time-stepping method with second-order integration accuracy using ideas from discrete mechanics. We treat only the case of perfectly inelastic collisions, however extension to the elastic case is possible along the same lines used in existing time-stepping schemes [2].

4.1 Interpenetration and Complementarity

Interpenetration must not occur between rigid bodies. Mathematically, this constraint can be expressed as an inequality,

$$\phi(q) \geq 0, \tag{17}$$

where $\phi(q)$ is a vector-valued function that evaluates the signed distance between closest points on all pairs of bodies.

To build a variational integrator that respects the interpenetration constraint, we add it to (10) with a corresponding Lagrange multiplier, γ [12]:

$$\delta \sum_{k=0}^{N-1} \mathscr{L}_d(q_k, q_{k+1}) + \gamma_k^T \phi(q_{k+1}) + \sum_{k=0}^{N-1} \frac{1}{2} F_d(q_k, q_{k+1}) \cdot (\delta q_k + \delta q_{k+1}) = 0. \tag{18}$$

Note the choice of time indices in the constraint term $\gamma_k^T \phi(q_{k+1})$ to indicate that a contact impulse during timestep k must be generated such that the *next* state satisfies the inequality $\phi(q_{k+1}) \geq 0$.

Following the same steps used to derive equation (16) in the previous section, we find,

$$
\begin{aligned}
D_2 \mathscr{L}_d(q_{k-1}, q_k) &+ D_1 \mathscr{L}_d(q_k, q_{k+1}) \\
&+ \frac{1}{2} F_d(q_{k-1}, q_k) + \frac{1}{2} F_d(q_k, q_{k+1}) + N(q_{k+1})^T \gamma_k = 0,
\end{aligned}
\tag{19}
$$

where $N(q)^T = (\partial \phi / \partial q)^T$ is the Jacobian mapping normal contact forces into generalized coordinates. In addition, solutions to (19) must satisfy the following conditions:

$$\gamma_k \geq 0$$
$$\phi(q_{k+1}) \geq 0 \qquad (20)$$
$$\gamma_k^T \phi(q_{k+1}) = 0.$$

The combination of (19) and (20) form the first-order necessary conditions, known as Karush-Kuhn-Tucker (KKT) conditions, for an inequality constrained optimization problem [4].

Physically, the Lagrange multiplier γ_k takes on the magnitude of the contact impulse in the normal direction. The three conditions in (20) are collectively known as a *complementarity constraint*. In addition to preventing interpenetration, they ensure that contact forces can only push bodies apart (not pull them together), and that contact forces can only act when bodies are in contact. Such constraints are commonly denoted using the following shorthand notation:

$$0 \leq \gamma_k \perp \phi(q_{k+1}) \geq 0. \qquad (21)$$

Intuitively, complementarity constraints express discontinuous "switching" behavior: only one variable or the other is allowed to be non-zero at a time. They are an inherent feature in many models of contact physics.

4.2 Coulomb Friction

Coulomb friction exerts forces in the plane tangent to the contact surface between two bodies. It can be described by the *Maximum Dissipation Principle* [16], which states that friction forces instantaneously maximize the dissipation of kinetic energy. Mathematically, this can be written as,

$$\begin{aligned} \underset{b}{\text{minimize}} \quad & \dot{q}^T D^T b \\ \text{subject to} \quad & \|b\| \leq \mu\gamma, \end{aligned} \qquad (22)$$

where b is the friction force, μ is the friction coefficient, D^T is the Jacobian mapping tangential contact forces into generalized forces, and the constraint ensures that forces remain within the Coulomb friction cone.

For computational reasons, it is standard in time-stepping methods to form an inner approximation to the friction cone using a polyhedron [24, 2]. For the special case of a pyramidal approximation, this is accomplished by defining a new friction vector β with twice as many elements as b, enforcing the constraint $\beta \geq 0$, and forming a new Jacobian matrix:

$$P = \begin{bmatrix} D \\ -D \end{bmatrix}. \qquad (23)$$

With this approximation, the optimization problem (22) becomes,

$$\underset{\beta}{\text{minimize}} \quad \dot{q}^T P^T \beta$$

$$\text{subject to} \quad \mu\gamma - e^T \beta \geq 0 \tag{24}$$

$$\beta \geq 0$$

where e is a vector of ones.

The set of first-order necessary conditions (KKT conditions) for an optimum of (24) are,

$$P\dot{q} + \psi e - \eta = 0$$

$$\beta, \psi, \eta \geq 0$$

$$\mu\gamma - e^T \beta \geq 0 \tag{25}$$

$$\psi^T \left(\mu\gamma - e^T \beta\right) = 0$$

$$\eta^T \beta = 0,$$

where ψ and η are Lagrange multipliers. In the more compact shorthand notation introduced in the previous subsection, these conditions can be rewritten as:

$$P\dot{q} + \psi e - \eta = 0$$

$$0 \leq \psi \perp \left(\mu\gamma - e^T \beta\right) \geq 0 \tag{26}$$

$$0 \leq \eta \perp \beta \geq 0.$$

Physically, the Lagrange multiplier ψ approximates the projection of the system's velocity onto the plane tangent to the contact manifold. The conditions in (26) ensure that the friction force will assume whatever value is necessary to prevent sliding when $\psi = 0$, up to the boundary of the friction cone. In the sliding case, when $\psi \neq 0$, the friction force will lie on the boundary of the friction cone.

4.3 A Second-Order Variational Time-Stepping Method

We now build a complete time-stepping method by combining the results of sections 4.1 and 4.2. We first define a vector λ that combines the normal and friction components of the contact impulse,

$$\lambda = \begin{bmatrix} \gamma \\ \beta \end{bmatrix}, \tag{27}$$

and the corresponding Jacobian matrix to map λ into generalized coordinates:

$$J = \begin{bmatrix} N \\ P \end{bmatrix}. \tag{28}$$

The discrete Euler-Lagrange dynamics can then be written as follows:

$$D_2 \mathscr{L}_d(q_{k-1}, q_k) + D_1 \mathscr{L}_d(q_k, q_{k+1})$$

$$+ \frac{1}{2} F_d(q_{k-1}, q_k) + \frac{1}{2} F_d(q_k, q_{k+1}) + J(q_{k+1})^T \lambda_k = 0. \quad (29)$$

The set of complementarity conditions derived in the previous subsections are used to determine λ_k in (29). Given q_{k-1} and q_k, the following feasibility problem can be solved to find λ_k and q_{k+1},

$$r(h, q_{k-1}, q_k, q_{k+1}, \lambda_k) = 0$$

$$P(q_{k+1}) \left(\frac{q_{k+1} - q_k}{h} \right) + \psi_k e - \eta_k = 0$$

$$0 \leq (\mu \gamma_k - e^T \beta_k) \perp \psi_k \geq 0 \qquad (30)$$

$$0 \leq \phi(q_{k+1}) \perp \gamma_k \geq 0$$

$$0 \leq \beta_k \perp \eta_k \geq 0,$$

where $r(h, q_{k-1}, q_k, q_{k+1}, \lambda_k) = 0$ refers to equation (29).

5 Direct Trajectory Optimization

We now propose a direct trajectory optimization algorithm that uses the variational time-stepping scheme developed in the previous section as a set of dynamics constraints. Our strategy is to formulate the trajectory optimization problem as a nonlinear program (NLP) and solve it using standard constrained optimization software.

To ease the numerical difficulties associated with complementarity constraints, we apply a smoothing scheme similar to that used in [7]. The key idea is to relax the equality constraints in the three complementarity conditions in (30) by replacing them with inequalities and introducing the slack variables s_k:

$$r(h, q_{k-1}, q_k, q_{k+1}, \lambda_k) = 0$$

$$P(q_{k+1}) \left(\frac{q_{k+1} - q_k}{h} \right) + \psi_k e - \eta_k = 0$$

$$\lambda_k, \psi_k, \eta_k, s_k \geq 0$$

$$\phi(q_{k+1}) \geq 0 \qquad (31)$$

$$(\mu \gamma_k - e^T \beta_k) \geq 0$$

$$s_k - \eta_k^T \beta_k \geq 0$$

$$s_k - \gamma_k^T \phi(q_{k+1}) \geq 0$$

$$s_k - \psi_k^T (\mu \gamma_k - e^T \beta_k) \geq 0.$$

Figure 1 illustrates the feasible regions for both the original "strict" complementarity constraints and the new relaxed complementarity constraints in (31). If the slack variables are reduced to zero, the two regions coincide.
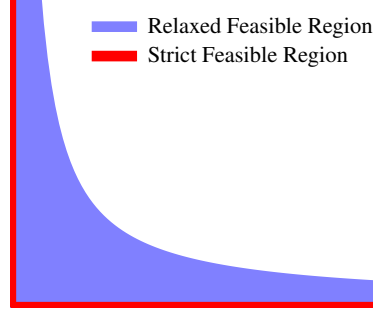

Fig. 1 Illustration of feasible regions for relaxed and strict complementarity constraints.

Physically, the relaxed complementarity constraints allow contact forces to act at a non-zero distance from the contact manifold. This aids convergence, but we would ultimately like solutions that closely respect the true constraints. To encourage convergence of solutions towards strict satisfaction of the complementarity constraints, we augment the cost function with a term that penalizes s_k. The trajectory optimization algorithm can now be stated as the following NLP:

$$
\begin{aligned}
\underset{h,\mathcal{Q},\mathcal{U},\mathcal{C}}{\text{minimize}} \quad & J(h,\mathcal{Q},\mathcal{U}) + \alpha \sum_{k=1}^{N-1} s_k \\
\text{subject to} \quad & f(h,q_{k-1},q_k,q_{k+1},\lambda_k,\psi_k,\eta_k) = 0 \\
& g(q_{k+1},\lambda_k,\psi_k,\eta_k,s_k) \geq 0 \\
& u_{min} \leq u_k \leq u_{max} \\
& h_{\min} \leq h \leq h_{\max},
\end{aligned}
\tag{32}
$$

where J is a cost function; α is a positive scalar weighting parameter; f and g are the equality and inequality constraints in (31); $\mathcal{Q}$ is the set of all configuration knot points, q_k; $\mathcal{U}$ is the set of all control inputs, u_k; and $\mathcal{C}$ is the set of all contact-related variables, λ_k, ψ_k, η_k, and s_k.

The penalty on the slack variables in the the cost function of (32) is a so-called "exact penalty" that has theoretical convergence guarantees with finite values of α [1]. In practice, we have observed good convergence behavior with modest values of α. Problem (32) can be solved with standard nonlinear programming algorithms like sequential quadratic programming (SQP) and interior-point methods [17]. It is also straight-forward to include additional constraints on the system's state and inputs.

6 Examples

To evaluate the proposed trajectory optimization algorithm, we demonstrate its ability to generate complex, multi-contact motions by optimizing walking trajectories for two simulated legged robots: Spring Flamingo and LittleDog. We also compare its accuracy to the first-order method used by Posa et al. [19] in both open- and closed-loop simulations. In all cases, the optimizer was initialized with dynamically infeasible trajectories consisting of linear interpolation between initial and goal poses. No *a priori* information about contact forces or mode sequences was used.

6.1 Spring Flamingo

Spring Flamingo is an 18-state planar bipedal robot with actuated hips and knees and a passive spring ankle joint [8]. A trajectory optimization problem was defined in which the robot was required to move from an initial standing pose to a final standing pose translated to the left. The following cost function was minimized,

$$J = \sum_{i=1}^{N-1} 0.1(x_i - x_g)^T (x_i - x_g) + u_i^T u_i, \tag{33}$$

where x_g is the goal state. Figure 2 shows a sequence of frames taken from the optimized walking gait. The algorithm discovered an energetically efficient heel-toe gait that exploits the passive dynamics of the leg and ankle.
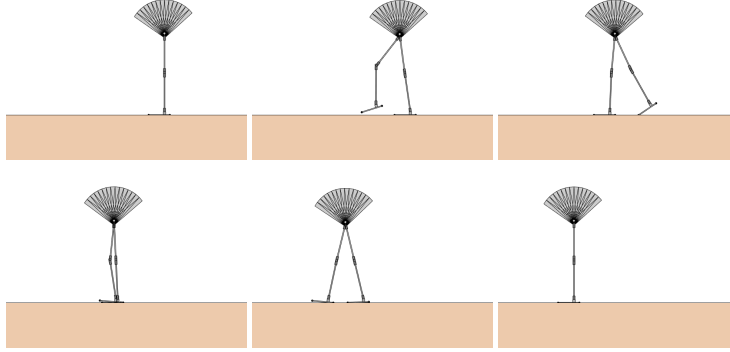

Fig. 2 Spring Flamingo optimized walking gait.

6.2 LittleDog

LittleDog is a 36-state quadrupedal robot designed by Boston Dynamics to enable research on legged locomotion [5]. A trajectory optimization problem was defined in which the robot was required to climb up an 11 cm step. Once again, initial and final state constraints were enforced and a simple quadratic cost function was minimized. Figure 3 shows an example climbing strategy and Figure 4 shows the corresponding sequence of modes (combinations of foot contacts) that were generated implicitly by the solver.
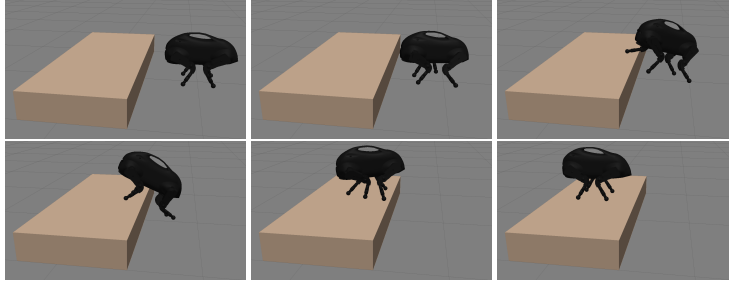
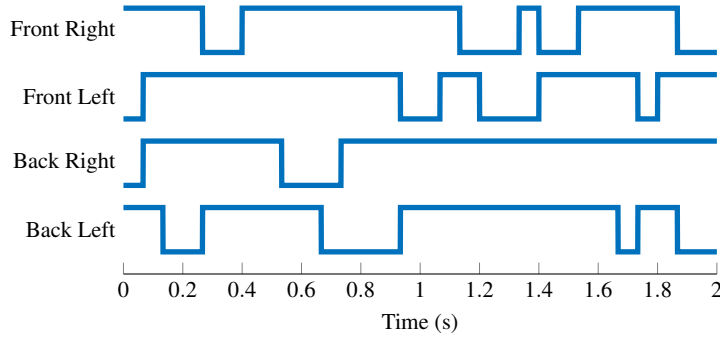
Fig. 3 LittleDog climbing a step.

Fig. 4 Contact mode sequence for each foot from LittleDog step-climbing example.

6.3 Simulation Accuracy

We compare the first-order and variational time-stepping methods in open-loop simulations of a tumbling brick hitting the ground and closed-loop simulations of

the LittleDog robot tracking a walking trajectory with proportional-derivative (PD) feedback control applied to its joints.
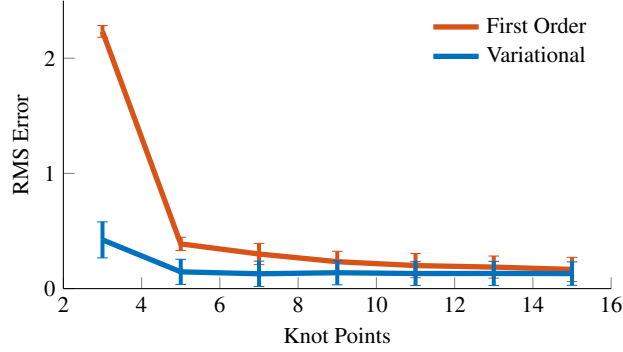

Fig. 5 Falling brick simulation RMS error and standard deviation

Tumbling-brick simulations were initialized with twenty different randomly chosen initial conditions while varying the number of knot points. A reference solution was computed using the first-order method at a sample rate of 2 kHz. Figure 5 shows the root mean square (RMS) error (compared to the reference solution) as a function of the number of knot points. The variational method achieves better accuracy with fewer knot points than the first-order time-stepping method.

To test closed-loop tracking performance, a set of walking trajectories was first optimized using both first-order and variational time-stepping dynamics as constraints. The number of knot points used to parameterize the trajectories was varied between 10 and 40. Simple PD control was applied to each joint of the robot, and simulations were performed using the first-order method at a sample rate of 2 kHz. Figure 6 shows the RMS tracking error in the robot's state. Once again, better accuracy is achieved with fewer knot points using the variational method.

7 Conclusions

We have presented a new family of variational time-stepping algorithms that generalize previous methods to higher orders of integration accuracy. We derived a second-order method and incorporated it into a direct trajectory optimization algorithm that solves for contact forces along with state and input trajectories. Our numerical tests suggest that the method offers improvements over existing first-order contact-implicit trajectory optimization algorithms, allowing smaller NLPs to be solved while maintaining reasonable accuracy. We also demonstrated the algorithm's ability to generate walking trajectories for simulated underactuated robots with minimal problem-specification effort.
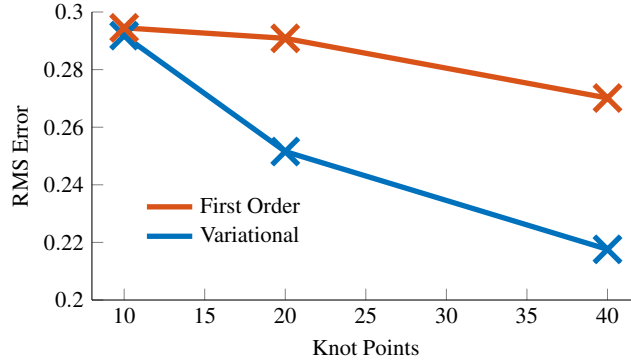
Fig. 6 RMS tracking error for LittleDog walking with PD tracking controller.

There are several directions for future work. First, a more extensive numerical comparison including 3rd and 4th-order time-stepping methods would allow us to better understand the trade-off between accuracy and computational cost. Second, our current MATLAB implementation requires several minutes to compute the SpringFlamingo and LittleDog plans described in the previous section. Significant speed improvements could be made with a careful C++ implementation that exploits the sparsity structure of the problem. Finally, as other authors have observed [15], the contact mode trajectory often changes over longer timescales than the state and input trajectories. Explicitly encoding this into the NLP formulation could aid convergence and avoid unnecessary contact transitions.

8 Acknowledgements

References

1. Anitescu, M.: On Using the Elastic Mode in Nonlinear Programming Approaches to Mathematical Programs with Complementarity Constraints. SIAM Journal on Optimization **15**(4), 1203–1236 (2005). DOI 10.1137/S1052623402401221
2. Anitescu, M., Potra, F.A.: Formulating dynamic multi-rigid-body contact problems with friction as solvable linear complementarity problems. Nonlinear Dynamics **14**(3), 231–247 (1997)
3. Betts, J.T.: Survey of Numerical Methods for Trajectory Optimization **21**(2), 193–207 (March–April 1998)
4. Boyd, S., Vandenberghe, L.: Convex Optimization. Cambridge University Press (2004)

5. Buchli, J., Pratt, J., Roy, N., Murphy, M.P., Saunders, A., Moreira, C., Rizzi, A.A., Raibert, M.: The LittleDog robot. The International Journal of Robotics Research **30**(2), 145–149 (2010). DOI 10.1177/0278364910387457
6. Buss, M., Hardt, M., Kiener, J., Sobotka, M., Stelzer, M., von Stryk, O., Wollherr, D.: Towards an Autonomous, Humanoid, and Dynamically Walking Robot: Modeling, Optimal Trajectory Planning, Hardware Architecture, and Experiments. In: Proceedings of the 3rd International Conference on Humanoid Robotics, pp. 2491–2496 (2003)
7. Fletcher, R., Leyffer, S.: Solving mathematical programs with complementarity constraints as nonlinear programs. Optimization Methods & Software **19**(1), 15–40 (2004)
8. J. Pratt, G. Pratt: Intuitive control of a planar bipedal walking robot. In: Proceedings. 1998 IEEE International Conference on Robotics and Automation (Cat. No.98CH36146), vol. 3, pp. 2014–2021 vol.3 (1998). DOI 10.1109/ROBOT.1998.680611
9. M. Neunert, F. Farshidian, A. W. Winkler, J. Buchli: Trajectory Optimization Through Contacts and Automatic Gait Discovery for Quadrupeds. IEEE Robotics and Automation Letters **2**(3), 1502–1509 (2017). DOI 10.1109/LRA.2017.2665685
10. M. Neunert, F. Farshidian, J. Buchli: Efficient whole-body trajectory optimization using contact constraint relaxation. In: 2016 IEEE-RAS 16th International Conference on Humanoid Robots (Humanoids), pp. 43–48 (15-17 Nov. 2016). DOI 10.1109/HUMANOIDS.2016. 7803252
11. Marsden, J., Ratiu, T.: Introduction to Mechanics and Symmetry, 2 edn. Texts in Applied Mathematics. Springer, New York (1999)
12. Marsden, J.E., West, M.: Discrete Mechanics and Variational Integrators. Acta Numerica **10**, 357–514 (2001)
13. Mayne, D.Q.: A second-order gradient method of optimizing non- linear discrete time systems. Int J Control **3**, 8595 (1966)
14. Mombaur, K.D.: Using optimization to create self-stable human-like running. Robotica **27**(3), 321–330 (2009). DOI 10.1017/s0263574708004724
15. Mordatch, I., Todorov, E., Popović, Z.: Discovery of complex behaviors through contact-invariant optimization. ACM Transactions on Graphics (TOG) **31**(4), 43–43:8 (2012). DOI 10.1145/2185520.2185539
16. Moreau, J.: On unilateral constraints, friction and plasticity. In: New Variational Techniques in Mathematical Physics, pp. 172–322. Springer (1973)
17. Nocedal, J., Wright, S.J.: Numerical Optimization, 2nd edn. Springer (2006)
18. Ober-Blobaum, S., Saake, N.: Construction and analysis of higher order Galerkin variational integrators. Advances in Computational Mathematics **41**, 955–986 (2015)
19. Posa, M., Cantu, C., Tedrake, R.: A direct method for trajectory optimization of rigid bodies through contact. International Journal of Robotics Research **33**(1), 69–81 (2014)
20. Posa, M., Kuindersma, S., Tedrake, R.: Optimization and stabilization of trajectories for constrained dynamical systems. In: Proceedings of the International Conference on Robotics and Automation (ICRA), pp. 1366–1373. IEEE, Stockholm, Sweden (2016)
21. Remy, C.D.: Optimal Exploitation of Natural Dynamics in Legged Locomotion. Ph.D. thesis, ETH ZURICH (2011)
22. Schultz, G., Mombaur, K.: Modeling and Optimal Control of Human-Like Running. IEEE/ASME Transactions on Mechatronics **15**(5), 783–792 (2010)
23. Stewart, D.E.: Rigid-body dynamics with friction and impact. SIAM review **42**(1), 3–39 (2000)
24. Stewart, D.E., Trinkle, J.C.: An implicit time-stepping scheme for rigid body dynamics with inelastic collisions and coulomb friction. International Journal for Numerical Methods in Engineering **39**(15), 2673–2691 (1996)
25. Tassa, Y., Erez, T., Todorov, E.: Synthesis and Stabilization of Complex Behaviors through Online Trajectory Optimization. In: IEEE/RSJ International Conference on Intelligent Robots and Systems (2012)
26. Todorov, E.: A convex, smooth and invertible contact model for trajectory optimization. In: Proceedings of the International Conference on Robotics and Automation (ICRA) (2011)
27. Xi, W., Remy, C.D.: Optimal Gaits and Motions for Legged Robots. In: Proceedings of the IEEE/RSJ International Conference on Intelligent Robots and Systems (IROS) (2014)